Iranian Journal of Geophysics, 2020, Page 79 - 92

Estimation of Source Location Using Curvature Analysis

Mohammad Barazesh [1]*and* Seyed-Hani Motavalli-Anbaran [2]

[1] *M.Sc. Student, Institute of Geophysics, University of Tehran, Tehran, Iran*
[2] *Assistant Professor, Institute of Geophysics, University of Tehran, Tehran, Iran*

(Received: 15 October 2019, Accepted: 18 February 2020)

Abstract

A quadratic surface can be fitted to potential-field data within 3×3 windows, which allow us to calculate curvature attributes from its coefficients. Phillips (2007) derived an equation depending on the most negative curvature to obtain the depth and structural index of isolated sources from peak values of special functions. They divided the special functions into two categories: Model-specific special functions (including Horizontal Gradient Magnitude (*HGM*) and absolute value) and Model-independent special functions (including Local Wavenumber (*LW*) and Total Gradient (*TG*)). We used the normalized source strength (*NSS*) as a new model-independent special function to estimate depth and shape factor of gravity and magnetic sources. It has its peak directly over the potential field sources (even for dipping sources), and is independent of magnetization direction in magnetic cases. Spurious results are removed by applying a threshold on the shape index attribute and the shape factor.

In this study, the method has been applied on noisy and noise-free synthetic models. For depth estimation of complex sources, we first estimated the depth and structural index from local wavenumber special function. Then, it was used as input to *TG* and *NSS* special functions. Finally, this method was tested on real data from Safoo Manganese ore, Northwest of Iran.

Keywords: Potential field, Curvature attributes, Special function

*Corresponding author: Barazeshm@ut.ac.ir

1 Introduction

To date, many automated techniques have been designed to quickly estimate source parameters of magnetic and gravity anomalies. Salem *et al*. (2005) obtained locations of the 2D magnetic source by solving a linear equation depending on local wavenumbers in the *x* and *z* directions. Beiki and Pedersen (2010) introduced a method to estimate source parameters by using eigenvectors of gravity gradient tensor data. Beiki (2010) showed that directional analytic signal satisfies the homogenous Euler deconvolution equation. He simultaneously calculated the type and location of sources for a window with varying size located around the maxima of their function. Abbas and Fedi (2014) estimated depth and structural index by defining a scale function from different orders of partial derivatives, which is independent of the structural index. Hansen and De Ridder (2006) proposed a linear feature analysis based on the curvature of the total horizontal gradient of the total magnetic field.

Oruç *et al.* (2013) used the smallest eigenvalue of the curvature matrix to determine the edges of anomaly sources. This eigenvalue is equivalent to the most negative curvature attribute that was introduced by Roberts (2001) for a quadratic surface. Therefore, most positive and negative curvature attributes are useful in determining the edges of sources with positive and negative density contrast, respectively. Some of these attributes are used to determine the boundaries of gravity sources by Barazesh *et al*. (2016). Phillips *et al*. (2007) introduced symmetrical special functions that have peaks above isolated sources in two categories to estimate the source parameters: a) *model-specific special functions:* such as Horizontal Gradient Magnitude (*HGM*) and the absolute value of a transformed observed field to locate specific sources with known shapes (e.g. sphere, horizontal line); b) *model-independent special functions:* such as Total Gradient (*TG*) and Local Wavenumber (*LW*) to determine some parameters of different types of anomaly sources. A quadratic surface should be fitted to a special function within 3×3 windows to calculate location and structural index of anomalous sources from the curvature and the special function value at peak location. In this paper, we added the normalized source strength to model-independent special functions introduced by Phillips *et al*. (2007), which are more effective than the *TG* and *LW* special functions. In addition, the shape factor can be calculated from it.

In this paper, first, a short description of the principle of the curvature method is presented. Then, this method was tested on gravity and magnetic models. Finally, the curvature analysis is applied on gravity data from Safoo Manganese ore.

2 Materials and Methods

2-1 Curvature attributes

Near massive bodies, the potential field is severely curved. Curvature is a curve property, which determines the amount of deviation from a straight line at any point. The standard formula to calculate the curvature of function *F(x)* in *x* direction is:

$$K = \frac{d^2F/dx^2}{(1+(dF/dx)^2)^{3/2}}. \quad (1)$$

For gridded data, we face with a surface having numerous curvatures at a certain point due to numerous intersection planes that can be introduced there. One expects the curvature has a maximum value perpendicular to the elongated direction, when the bodies are elongated in a direction. The most suitable curvature called “normal curvature” can be obtained from the intersection of planes that are perpendicular to the surface. Some of the most useful normal

curvatures are presented in Appendix A. A quadratic surface (Equation A1) is fitted to the data (or special functions) within 3×3 windows and then curvature attributes can be calculated from the coefficients of this surface (Equations A2-4). The most positive curvature (Equation A2) and the most negative curvature (Equation A3) are calculated along and perpendicular to the strike of the source, respectively. Therefore, the most negative curvature is suitable for depth estimation.

2-2 Application of curvature attributes in depth estimation

The main idea in determination of source parameters is based on curvature analysis of certain special functions that have peaks over isolated sources. For gridded data, special functions at (x, y, z), over isolated sources, have the following general form:

$$S(x, y, z) = \frac{\alpha}{(X^2 + Y^2 + Z^2)^{\beta}}. \quad (2)$$

where $X = (x - x_0)$, $Y = (y - y_0)$, $Z = (z - z_0)$ and (x_0, y_0, z_0) are the source location. β is a positive constant, α is called geometry factor which depends on physical and geometrical properties of the source. Once the depth has been determined, the geometry factor can be estimated as follows:

$$\alpha = Z^{2\beta} \times S(x_0, y_0, z). \quad (3)$$

Finding the peak location of ridge crests, (x_0, y_0), is discussed in detail by Phillips *et al.* (2007) using curvature. The depth, *Z*, can be calculated in terms of the special function value and the most negative curvature at the peak location, (x_0, y_0), through the substitution of Equation (2) in (1),:

$$Z = \sqrt{-\frac{2\beta S(x_0, y_0, z)}{K_{neg}(x_0, y_0, z)}}. \quad (4)$$

Phillips *et al.* (2007) categorized the special functions, which have the form of Equation (2) over the anomaly, into two groups: *Model-specific special functions* and *model-independent special functions*. The first group includes *HGM (T)* (Equation 5) and *T* or the absolute value ($|T|$).

$$HGM = \sqrt{(\frac{\partial T}{\partial x})^2 + (\frac{\partial T}{\partial y})^2}. \quad (5)$$

T can be observed as a potential-field data (vertical components of the gravity vector or total magnetic intensity field) or a transformed version thereof. *HGM* can be used to calculate the depth of specific sources such as a contact, horizontal and vertical cylinder, etc. Some of these sources and their β values are presented by Phillips *et al.* (2007). The second group contains the Total Gradient (*TG*) and Local Wavenumber (*LW*), which are used to estimate the depth of a variety of sources:

$$TG(x, y) = \sqrt{\left(\frac{\partial T}{\partial x}\right)^2 + \left(\frac{\partial T}{\partial y}\right)^2 + \left(\frac{\partial T}{\partial z}\right)^2}, \quad (6)$$

(7)

$$LW(x, y) = \frac{\frac{\partial^2 T}{\partial x \partial z}\frac{\partial T}{\partial x} + \frac{\partial^2 T}{\partial y \partial z}\frac{\partial T}{\partial y} + \frac{\partial^2 T}{\partial z^2}\frac{\partial T}{\partial z}}{\left(\frac{\partial T}{\partial x}\right)^2 + \left(\frac{\partial T}{\partial y}\right)^2 + \left(\frac{\partial T}{\partial z}\right)^2}.$$

A structural index must be assumed to estimate the depth (Equation 4) from *TG*, but in the case of *LW* (for which $\beta = 1$) the structural index can be estimated from the calculated depth (Equation 4) as follows:

$$SI_{est} = -LW(x_0, y_0) Z_{est} - 1. \quad (8)$$

where SI_{est} and Z_{est} are the estimated structural index and depth, respectively. Phillips (2007) designed an extension as

Geosoft executable to implement depth estimation method using curvature.

We use the normalized source strength (*NSS*) (Equation 9) as the third model-independent special function:

$$NSS = \sqrt{-\lambda_2^{\,2} - \lambda_1 \lambda_3}. \qquad (9)$$

where $\lambda_i\,(i = 1,2,3)$ are eigenvalues of the gradient tensor (Γ),

$$\Gamma = \begin{pmatrix} T_{xx} & T_{xy} & T_{xz} \\ T_{xy} & T_{yy} & T_{yz} \\ T_{xz} & T_{yz} & T_{zz} \end{pmatrix}. \qquad (10)$$

$T_{\alpha\beta}\,(\alpha,\beta = x, y, z)$ are components of the gravity or magnetic gradient tensor. The normalized source strength of simple sources has the form of Equation 2,

$$NSS(x, y, z) = \frac{q\sigma}{(X^2 + Y^2 + Z^2)^{\frac{SI+1}{2}}}. \qquad (11)$$

where q, the shape factor, depends on the physical and geometrical properties of the model (Table 1), $\sigma = C_m$ (10^{-7} *H/m*) or *G* for magnetic and gravity sources, respectively (Table 1). Therefore, q can be calculated using

$$q = \frac{Z^{SI+1}\, NSS(x_0, y_0, z)}{\sigma}.$$

The components of the third column of the gradient tensor are Hilbert transform pairs of the first and second columns. To calculate the components of the gravity gradient tensor, we used the method introduced by Mickus and Hinojosa (2001). The components of magnetic gradient tensor are calculated as described by Schmidt and Clark (1998) in the Fourier domain. As total gradient special function (*TG*), it is necessary to assume a structural index (*SI*) and then $\beta = \frac{SI+1}{2}$ (Table 1) to estimate the depth (Equation 4) from *NSS* special function. This indicates that the *NSS* is an appropriate alternative to the total gradient for purposes of depth estimation.

The shape index attribute (*SHI*) (Equation A4) is defined as an angle in the $(K_{neg}+K_{pos})\times(K_{neg}+K_{pos})$ plane and numerically determines the shape of surface *S*. The *SHI* changes from -1 (spherical cup) and +1 (spherical cap) and by going from the positive sign to the negative sign, the surface shape changes from being concave (concave downward)

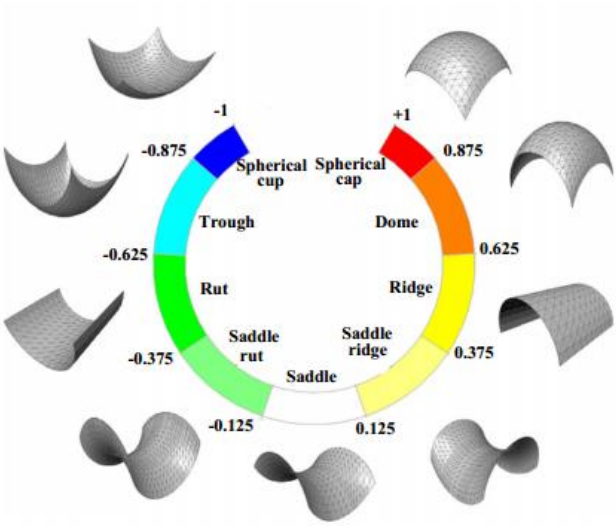

Figure 1. Classification of the local shape of the surface in terms of shape index (SHI) values (after Xú et al.).

Table 1. Normalized source strength (NSS) special function for gravity (Grav) and magnetic (Mag) sources that has the form of Equation 2.

ρ = density contrast, J= magnetization intensity (A/m), M= excess mass of sphere (kg), V= volume of sphere, m= mass per unit length of the line source, C=100 nH/m t= perpendicular thickness of the sheet, m_L is linear density of effective dipole moment and G= gravitational constant .

Gravity/Magnetic source	*NSS (Grav)*	*NSS (Mag)*	$\beta(grav/mag)$
Sphere	$NSS=\frac{GM}{(X^2+Y^2+Z^2)^{3/2}}(q=M)$	$NSS=\frac{3C_mJV}{(X^2+Y^2+Z^2)^2}(q=3JV)$	1.5/2
Horizontal cylinder	$NSS=\frac{2Gm}{X^2+Y^2+Z^2}(q=2m)$	$NSS=\frac{4C_mm_L}{(X^2+Y^2+Z^2)^{3/2}}(q=4m_L)$	1/1.5
Thin sheet	$NSS=\frac{2G\rho t}{(X^2+Y^2+Z^2)^{1/2}}(q=2\rho t)$	$NSS=\frac{2C_mJ't}{X^2+Y^2+Z^2}(q=2J't)$	0.5/1

to convex (concave upward). A classification of the surface shape with *SHI* values is shown in Figure 1. Barraud (2013) showed that *SHI* is a suitable criterion for removing incorrect depth estimates of model-specific special functions that do not satisfy the 2D condition (it should be noted that in this paper, the concepts of the three parameters of the shape index attribute (*SHI*), the structural index (*SI*) and the shape factor (*q*) are completely different). The special functions (*S*) form the ridge-like surface over the anomaly sources. Therefore, *SHI* is a suitable criterion for removing extra and spurious solutions. Since the model-independent special functions have locally shapes (e.g. over the edges of anomaly sources) have shapes like ridges ($0.375 \le SHI \le 0.625$), we can also apply this criterion to remove incorrect depth, structural index and shape factor from these special functions (of course, this interval can be changed depending on the local shape of the surface).

3 Synthetic data example

We applied the above-mentioned method to a dipping prism (300m×300m×200m) which carries a remanent magnetization with a Koenigsberger ratio (Q) equal to 2.5 and depth to top of 20 m. The induced and remanent magnetization vectors, (inclination, declination), are (-60°, 0) and (-20°, -20°), respectively. The geomagnetic field intensity was 28,000 nT. Figure 2 shows a 3D view of the dipping prism. Figures 3a-c show the magnetic field and the calculated total gradient and normalized source strength of the dipping prism, respectively.

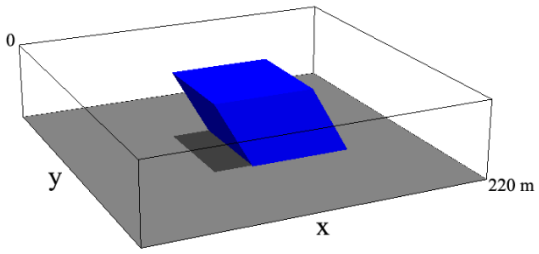

Figure 2. A 3D view of a prism model with dip of 60°.

As seen from Figure 3c, the maximum of *NSS* is located on the true edges and shows the low sensitivity to the magnetization direction in comparison with the total gradient. To estimate the source parameters, first we apply the *LW* special function to calculate the depth (Equation 4) and structural index (Equation 8) from the model of Figure 2. We used the following criteria to remove the spurious solutions from *LW* special functions:

1. Solutions with negative depths,
2. Solutions with unreasonable structural index,
3. Solutions outside of $0.375 \leq SHI \leq 0.625$.

Figure 4a shows the depths obtained from the *LW* special function. Because of using second-order derivatives in *LW*, this function has created dispersed solutions outside the prism location. Depths are not well-resolved in the corners of the prism as the *LW* special function does not fulfill the 2D condition and does not exhibit a ridge-like shape in the corners. The structural indices shown in Figure 4b are very close to zero, which is the theoretical structural index of a magnetic contact model.

To estimate the depth of the prism (Equation 4) from the total gradient special function, the estimated *SI* from the local wavenumber function over the edges ($SI = 0$ or $\beta = 0.5$) is assumed as input (Figure 4c). The depth values from *TG* are very close to the results of the *LW*, except on the western edge of the cube and the corners. Applying *SHI* criterion plus removing negative depths, we have tried to remove the spurious solutions (*TG* uses two criteria, whereas the local wavenumber special function uses three criteria).

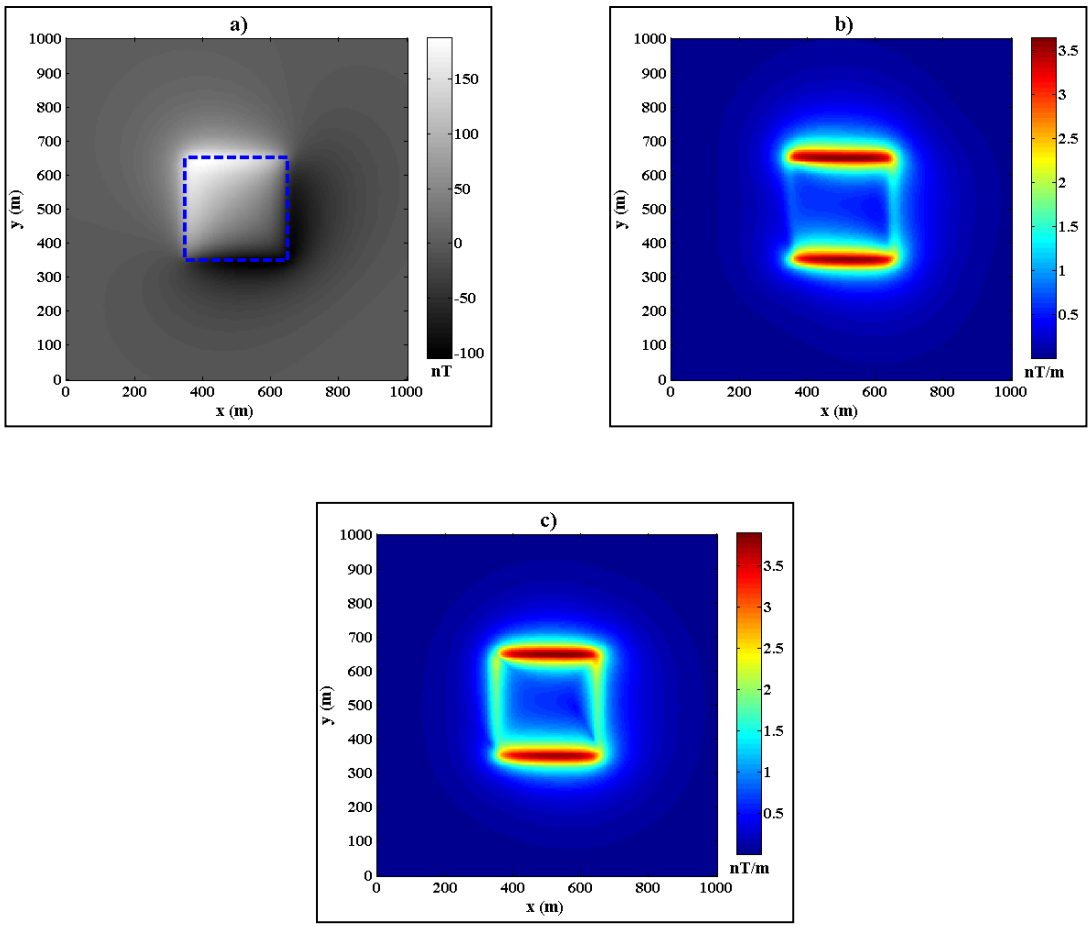

Figure 3. a) Synthetic magnetic anomaly for the body whose outline is shown with the dashed line. The body had a depth to top 20 m and induced and remanent magnetization vector, (inclination, declination), are (-60°, 0) and (-20°, -20), respectively. The body had 200 m depth extent, a susceptibility of 0.01 SI units with Koenigsberger ratio 2.5. The grid spacing was 5 m. The geomagnetic field intensity was 28,000 nT. b) Total gradient (TG) special function of the data from panel (a). c) Normalized source strength (NSS) special function of the data from panel (a).

The *NSS* special function was obtained from the eigenvalues of the magnetic gradient tensor. We use Equation 4 to calculate depth by assuming he estimated structural index from *LW* special function (*SI* = 0 or β = 0.5). Figures 5a-b show the results of depth and shape factor, which are calculated from the *NSS* special function. Compared to *TG* and *LW* special functions, solutions of the normalized source strength are exactly over the prism boundaries, and spurious results disappear by applying *SHI* criteria.

The interference effect of the neighboring source is shown by considering a synthetic model involving two prisms that are located at different depths. Table 2 describes the physical and geometrical properties of the prisms. We have also added a random Gaussian noise, *N (0, σ^2)* with standard deviation equal to 2% of the standard deviation of each magnetic tensor components to the corresponding component. Figures 6a and 6b, respectively, show a 3D view of the synthetic model and depth solutions using the *NSS* special function after applying the *SHI* criterion. As in the previous model, we assumed β = 0.5 for this model to estimate the depth. The estimated depth over the edges is very close to the real values. Many spurious solutions have been removed by applying the *SHI* criterion. However, the spurious solutions have not been completely removed.

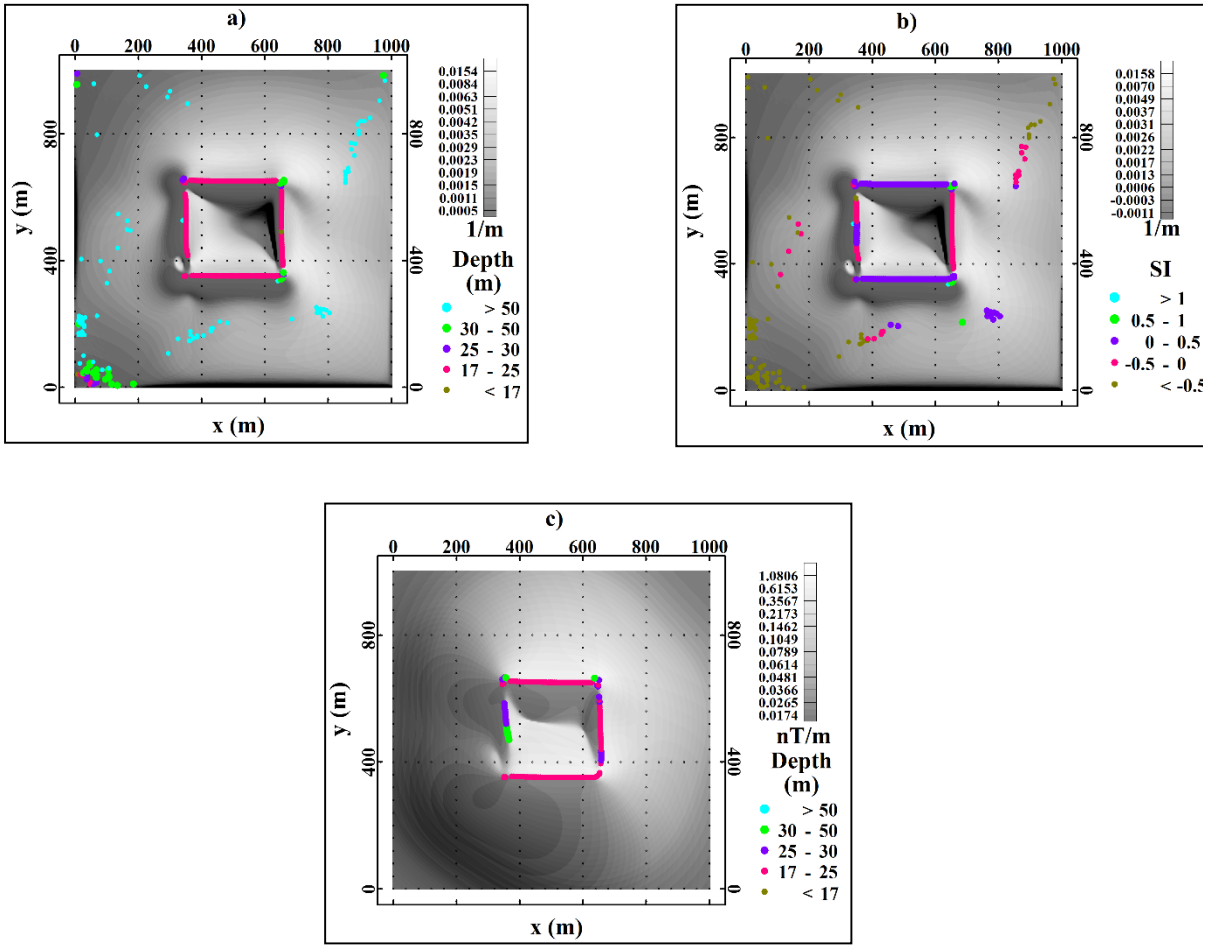

Figure 4. Special function results after applying the SHI criterion for synthetic model of Figure 2. a) Depth estimation from LW. b) Estimated structural index (SI) approximately equal to zero. c) Depth estimation from TG assuming $SI = 0$. Background map is corresponding special functions.

Table 2. Physical properties of prisms shown in Figure 6a.

Body	Depth to top (km)	Depth extent (km)	Width (km)	Magnetization (Inc, Dec)	Susceptibility (SI)	Q ratio
Prism 1	0.5	15	20	(-60˚, 0)	0.015	1.5
Prism 2	1	20	20	(-60˚, 0)	0.01	1

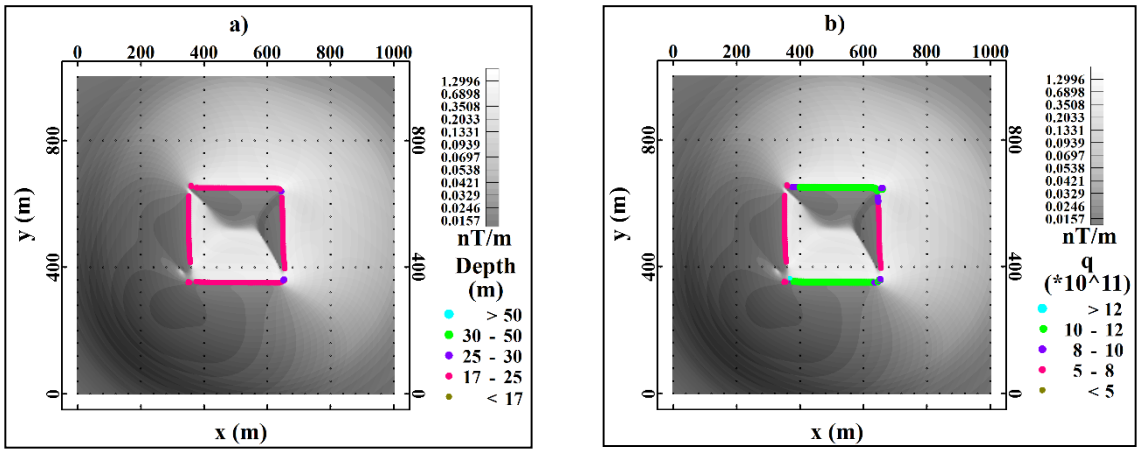

Figure 5. Results using the NSS special function after applying the SHI criterion for the synthetic model of Figure 2. a) Depth and b) shape factor. Background map shows the NSS special function of the dipping prism.

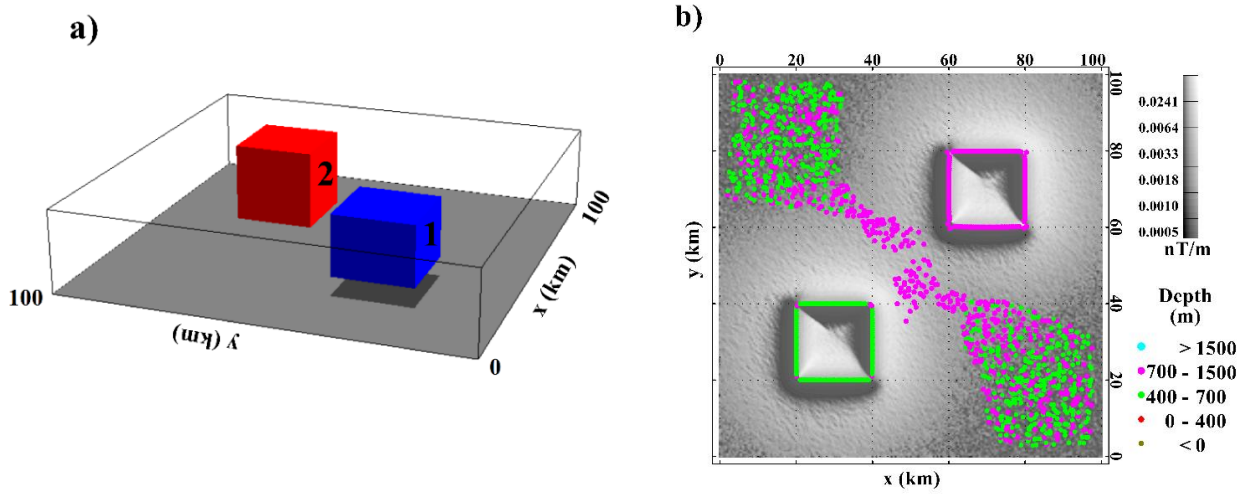

Figure 6. a) A 3D view of two prisms model. b) Depth using the NSS special function after applying the SHI criterion. Background map shows the NSS special function of the prisms.

As the last example, we considered a finite horizontal cylinder in the gravity field. The sensitivity of the method to the random noise was tested by estimating the source location and structural index in the presence of Gaussian noise with zero mean and standard deviation of +0.5μGal (Figure 7a).

We used an upward-continuation filter of 100 m before applying the method to reduce the effect of noise (Figures 7b and 7c). This was chosen equal to 150 m for

the *LW* special function (Figures 7d and 7e).

The gravity effect of the finite horizontal cylinder along the y-axis (from y_1 to y_2) can be derived as follows,

$$g_z = -\pi R^2 G\rho\,(z - z_0)\frac{\frac{y-y_1}{r_1} - \frac{y-y_2}{r_2}}{(x-x_0)^2 + (z-z_0)^2}. \quad (12)$$

where R is the radius (m), G is gravitational constant, ρ is the density contrast, and $r_i = \sqrt{(x-x_0)^2 + (y-y_i)^2 + (z-z_0)^2}, i = 1,2.$

In this case, we choose the gravity effect as a model-specific special function, assuming the infinite horizontal cylinder model (*SI*=1 or $\beta = 1$ (Table 2 in

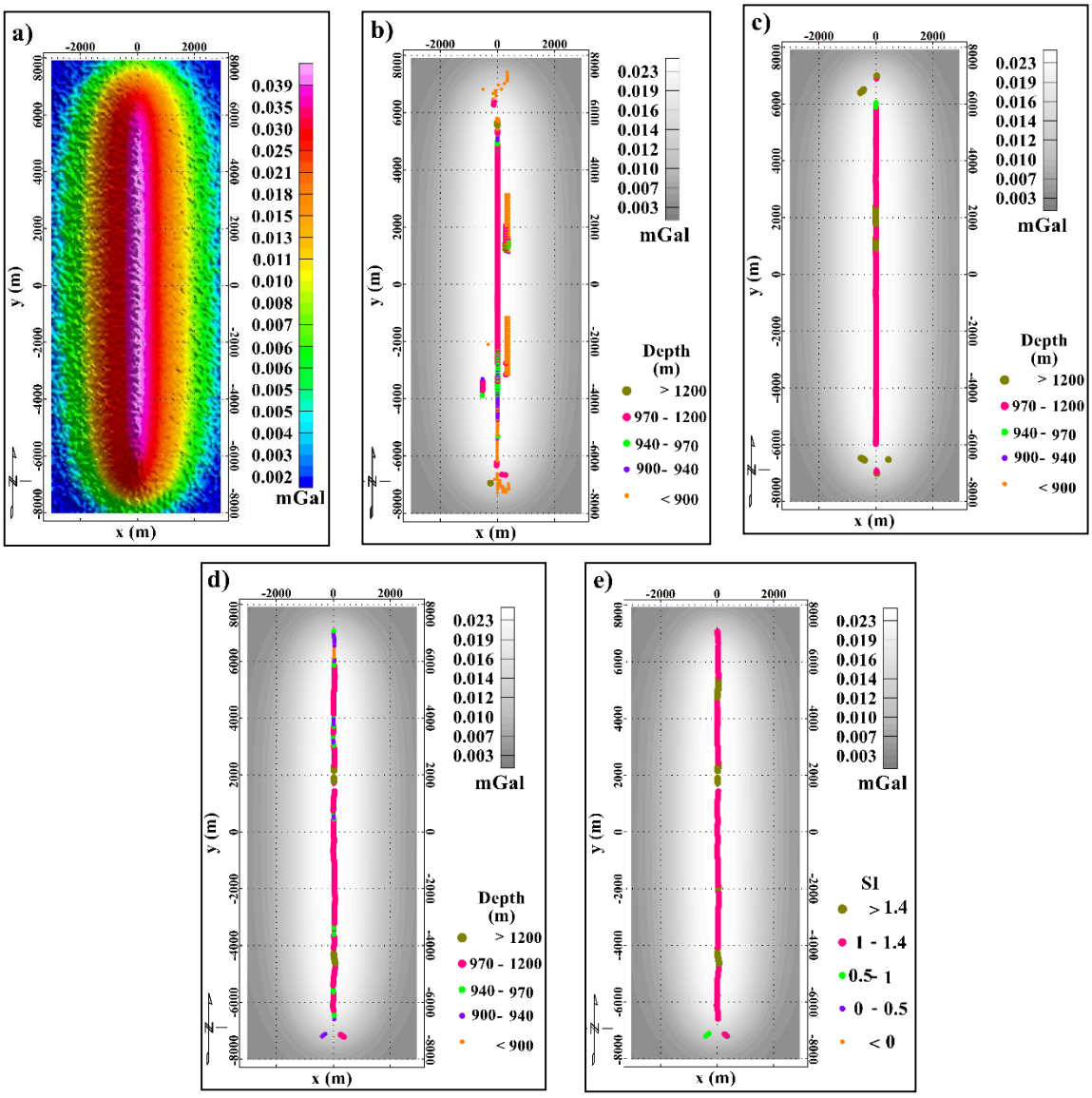

Figure 7. a) Gravity anomaly of the elongated cylindrical model (14 km) in the presence of Gaussian noise with zero mean and standard deviation of $\pm 0.5\mu$Gal . b) model-specific special function results assuming an infinite cylinder with SI=1. c) TG results assuming SI=1. d) LW results. e) Structural index (SI) calculated from LW. Background map shows gravity effect of the finite cylinder after upward continuation of 100 m.

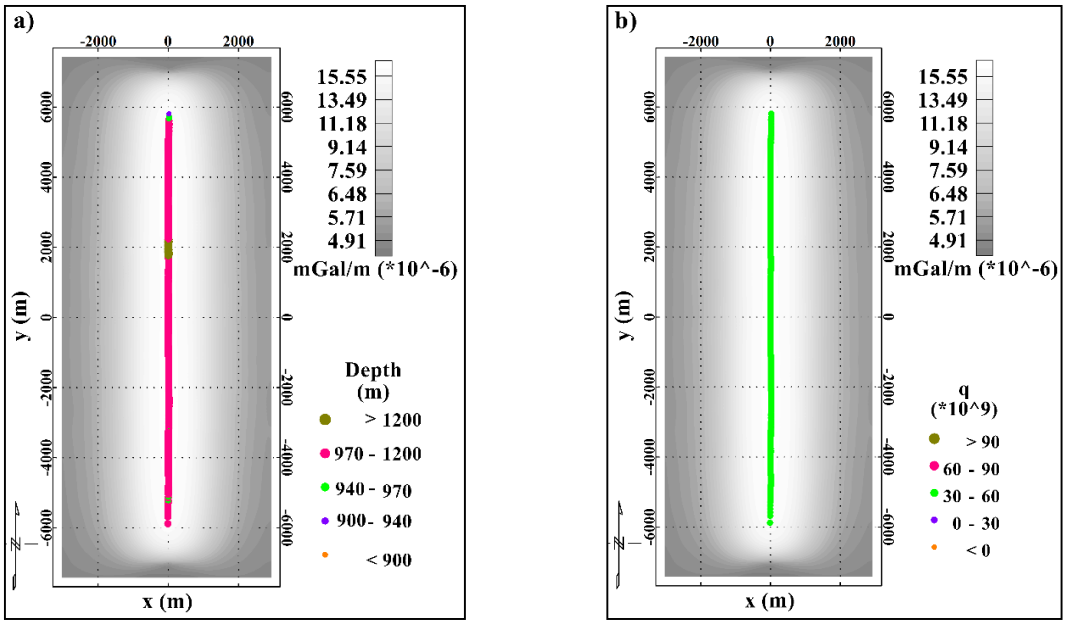

Figure 8. The NSS special function results after applying the SHI criterion for the synthetic model of Fig. 7a. a) Depth and b) shape factor. Background map shows NSS special function of the horizontal cylinder. Data were upward continued by 100 m before calculations.

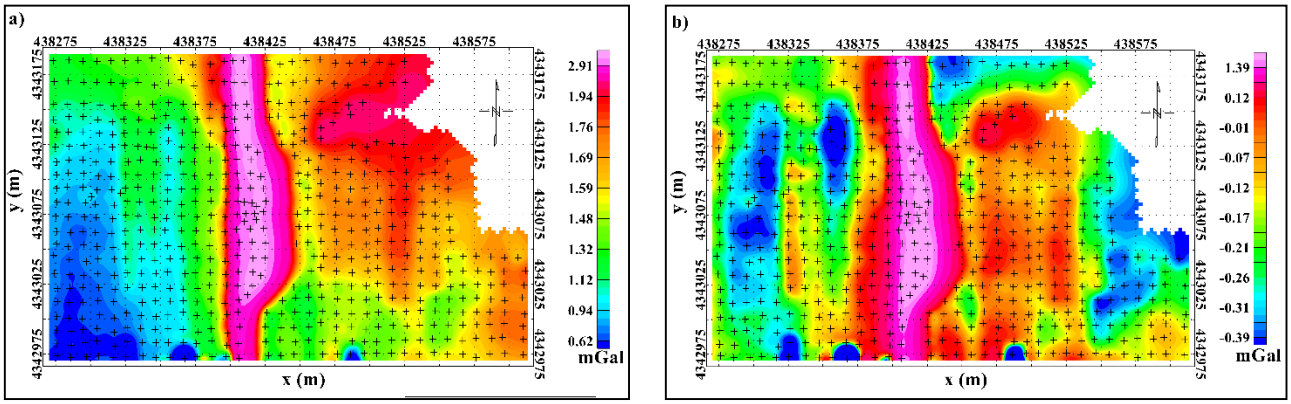

Figure 9. a) Bouguer gravity and b) residual anomaly map over the Safoo manganese ore superimposed on the location of stations (+symbols).

Phillips *et al.* (2007)) to calculate the depth from Equation 4 (Figure 7b). The resulting depths are in good agreement with the central depth of the horizontal cylinder. The estimated depths from the *TG* special function are shown in Figure 7c.

To compare the results of the *TG* with the results of model-specific special functions, a structural index of 1 was selected. The estimated depth from *TG* is very close to the depths obtained from model-specific special functions.

Figure 7d shows the depth estimated from *LW* special function. Using Equation 8, the structural index is estimated as being approximately equal to 1.2, which is very close to the theoretical structural index of an infinite horizontal cylinder model (Figure 7e). The *SHI* criterion was applied to remove spurious estimations from all special

function results. The estimated source locations and shape factor are superimposed on the calculated normalized source strength at 100 m above the observation level plotted in Figures 8a and 8b, respectively. From these figures, it can be observed that the estimated depths (Equation 4) from *NSS* are close to those of the other special functions assuming *SI*=1. It should be noted that upward continuation of 100 m was applied to the data before calculation of the *NSS* special function.

4 Field Example

The application of the curvature method to real gravity data is demonstrated on a data set from the Safoo manganese deposit, northwest of Iran. The objective is to locate the geological bodies using curvature analysis of special functions. Safoo manganese deposit is located about 25 km north of Chalderan city (Siyah Cheshmeh) and southwest of Maku, northwest of Iran. This area is placed structurally and geologically within the ophiolite zone in the northwest of Iran (known as the Khoy ophiolite). In the upper layers of the ophiolite and near the contact with pelagic limestones, deposits of manganese in various forms (e.g. lenticular, massive and strip-shaped) have been found. In Safoo area, manganese deposits are located within red calcareous pelagic shales and pelagic limestone. The mentioned rocks are cut by mafic dikes (diabase) in some parts. At least, three mineralized horizons were found; the largest of which is 50 m long and 5 m thick. The main mineralized resources are surrounded by pelagic rocks in different horizons. Geological information showed that manganese ore occurs at a depth of 3 m to 25 m.

Gravity data were collected on an approximately regular grid with a line spacing of 9 m and over the central anomaly about 5 m. Figure 9a shows the Bouguer gravity map superimposed on the location of stations. The residual anomaly was obtained by subtracting one-order trend from the Bouguer anomaly (Figure 9b). A relatively large anomaly elongated in north-south direction (near the center of the region) can be seen on Figures 9a and 9b. Data were interpolated to a grid using the minimum curvature algorithm. Curvature attributes were calculated using the method described above from the residual gravity anomaly.

Solutions with an unreliable structural index (*SI*) and *SHI* (solutions outside of $-1 \le SI \le 2$ and $0.375 \le SHI \le 0.625$) and a depth to source with negative values are rejected. Figure 10 shows results of source location and structural index using *LW* and *TG* special functions. The estimated structural index ($\cong 0.6$) (Figure 10b) is used as an input to *TG* (Figure 10c). The estimated depths to source for the central body are mainly between 5 m to 15 m, but the eastern edge is not well delineated by the total gradient and local wavenumber special functions. The gravity gradient tensor components are calculated as described by Mickus and Hinojosa (2001). Figure 11 shows that the *NSS* over the central anomaly enhances the eastern and western edges of the gravity source. The estimates of depths to source (Equation 4) and shape factor of causative bodies (by assuming $SI = 0.6$), superimposed on the *NSS* map, are plotted in Figure 11 (a and b), respectively. The clustered solutions along the edges of the central anomaly agree very well with geological information. The western and eastern edges of the central anomaly are well delineated by a set of solutions, and the depth is estimated about 6 m for both edges. The normalized source strength yields two positive ridges located approximately at the edges.

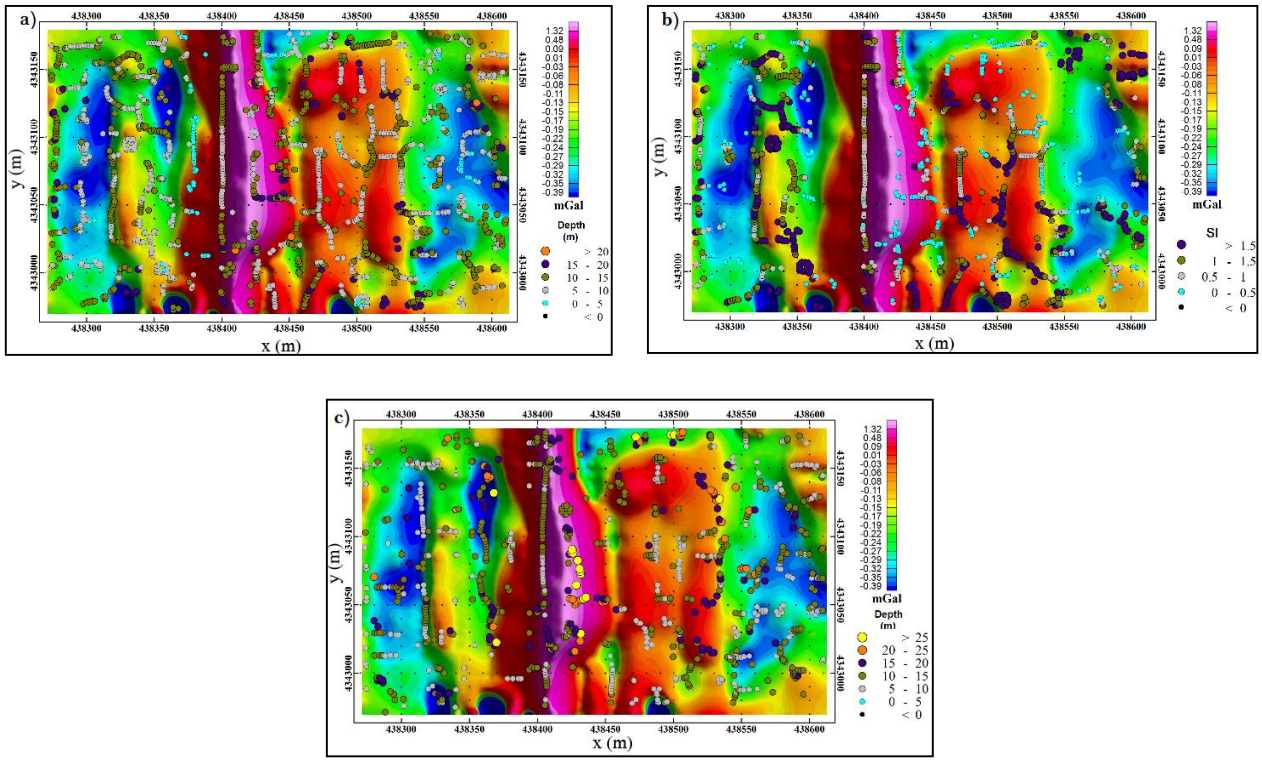

Figure 10. Special function results after applying the SHI criterion for Safoo manganese ore. a) Depth estimation from LW. b) Structural index ($SI \cong 0.6$). c) Depth estimation from TG assuming SI = 0.6. In these figures, background map is residual gravity anomaly.

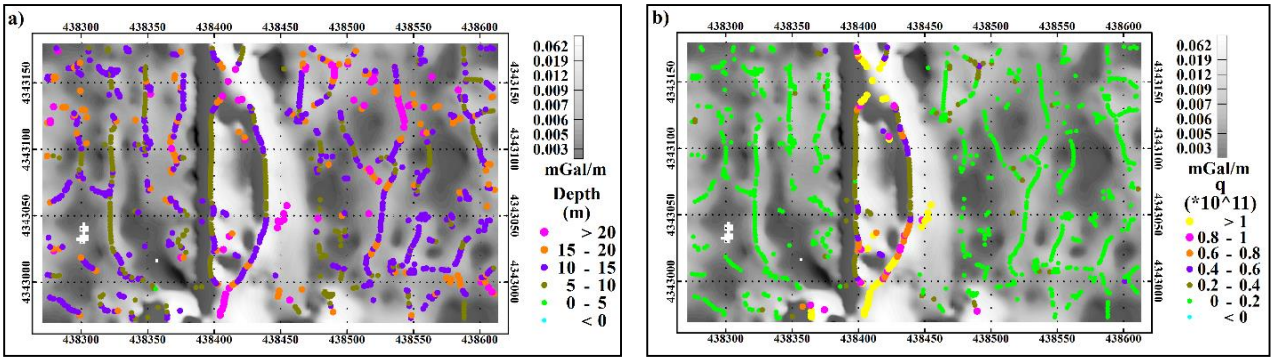

Figure 11. The NSS special function results after applying the SHI criterion for Safoo manganese ore. a) Depth and b) shape factor. Background map is NSS special function of Safoo deposit.

5 Results and Discussion

In this paper, we studied the curvature analysis of special functions for interpretation of potential field data. Phillips *et al.* (2007) fitted a quadratic surface in a least-squares sense to data within 3×3 windows. They showed that the source location and the structural index of sources can be estimated from special functions. We used normalized source strength (*NSS*) as a new model-independent special function, which enables us to obtain depth and shape factor for a variety of sources. This special function has maxima located exactly above the anomaly sources in

comparison with other special functions whose maxima have offset from edges in the presence of remanent magnetization. For an unknown source, first we use *LW* special function to determine the depth and the type of source (structural index). Then, the estimated structural index can be used as input to *TG* and *NSS* special functions to estimate depth, so that this strategy gives better results. The quality of obtained solutions can be evaluated by applying thresholds on the shape index attribute (*SHI*), the geometry factor (shape factor) and the estimated depth. This method was applied on noisy and noise-free gravity synthetic models. Finally, this method has been tested on the gravity data of Safoo manganese ore, and the results prove the advantage of the proposed method. Using curvature analysis as a complete package, we obtained a structural index and depth value from the local wavenumber special function over the eastern edge of the central anomaly. The estimated structural index was then used as input to total gradient and normalized source strength special functions to calculate the shape factor and depth. The normalized source strength exactly determined both eastern and western edges of the central anomaly plus depth and shape factor.

Acknowledgment

The authors would like to thank gravity department of Institute of Geophysics, University of Tehran, for permission to use their real gravity data from Safoo manganese ore. We would also like to thank Prof. Hermann Zeyen for his comments on the manuscript.

References

Salem, A., et al., Interpretation of magnetic data using an enhanced local wavenumber (ELW) method. Geophysics, 2005. **70**(2): p. L7-L12.

Beiki, M. and L.B. Pedersen, Eigenvector analysis of gravity gradient tensor to locate geologic bodies. Geophysics, 2010. **75**(6): p. I37-I49.

Beiki, M., Analytic signals of gravity gradient tensor and their application to estimate source location. Geophysics, 2010. **75**(6): p. I59-I74.

Abbas, M.A., M. Fedi, and G. Florio, Improving the local wavenumber method by automatic DEXP transformation. Journal of Applied Geophysics, 2014. **111**: p. 250-255.

Hansen, R.O. and e. deridder, Linear feature analysis for aeromagnetic data. Geophysics 71, L61–L67. doi: 10.1190/1.2357831, 2006.

Oruç, B., et al., Structural interpretation of the Erzurum Basin, eastern Turkey, using curvature gravity gradient tensor and gravity inversion of basement relief. . J. Appl. Geophys. 88, 105–113, 2013.

Roberts, A., Curvature attributes and their application to 3D interpreted horizons .First break, 2001. **19**(2): p. 85-100.

Barazesh, M., S.-H. Motavalli-Anbaran, and H. Ghorbanian, Application of surface-derived attributes in determining boundaries of potential-field sources. Iranian Journal of Geophysics, 2016. **9**(5): p. 57-71.

Phillips, J.D., R.O. Hansen, and R.J. Blakely, The use of curvature in potential-field interpretation*. Exploration Geophysics, 2007. **38**(2): p. 111-119.

Bergbauer, S., The Use Of Curvature For The Analyses Of Folding And Fracturing Withapplication To The Emigrant Gap Anticline,Wyoming. September 2002.

Barraud, J., Improving identification of valid depth estimates from gravity gradient data using Curvature and Geometry analysis. First break, Volum 31, April 2013.

Phillips, J.D., Geosoft eXecutables (GX's) developed by the US Geological Survey, version 2.0, with notes on GX development from Fortran code. 2007: US Geological Survey.

Clark, D.A., New methods for interpretation of magnetic vector and gradient tensor data I: eigenvector analysis and the normalised source strength. Exploration Geophysics, 2012. **43**(4): p. 267-282.

Beiki, M., et al., Estimating source location using normalized magnetic source strength calculated from magnetic gradient tensor data. Geophysics, 2012. **77**(6): p. J23-J38.

Beiki, M., P. Keating, and D.A. Clark, Interpretation of magnetic and gravity gradient tensor data using normalized source strength–A case study from McFaulds Lake, Northern Ontario, Canada. Geophysical Prospecting, 2014. **62**(5): p. 1180-1192.

Mikhailov, V., et al., Tensor deconvolution: A method to locate equivalent sources from full tensor gravity data. Geophysics, 2007. **72**(5): p. I61-I69.

Nabighian, M.N., Toward a three-dimensional

automatic interpretation of potential field data via generalized Hilbert transforms: Fundamental relations. Geophysics, 1984. **49**(6): p. 780-786.

Nabighian, M.N. and R. Hansen, Unification of Euler and Werner deconvolution in three dimensions via the generalized Hilbert transform. Geophysics, 2001. **66**(6): p .1805-1810.

Mickus, K.L. and J.H. Hinojosa, The complete gravity gradient tensor derived from the vertical component of gravity: a Fourier transform technique. Journal of Applied Geophysics, 2001. **46**(3): p. 159-174.

Schmidt, P.W. and D.A. Clark ,The calculation of magnetic components and moments from TMI: A case study from the Tuckers igneous complex, Queensland. Exploration Geophysics, 1998. **29**(3/4): p. 609-614.

Pedersen, L. and T. Rasmussen, The gradient tensor of potential field anomalies :Some. implications on data collection and data processing of maps. Geophysics, 1990. **55**(12): p. 1558-1566

Koenderink, J.J. and A.J. Van Doorn, Surface shape and curvature scales. Image and vision computing, 1992. **10**(8): p. 557-564.

Xú, S., et al ,.STEP-NC based reverse engineering of in-process model of NC simulation. The International Journal of Advanced Manufacturing Technology, 2016. **86**(9-12): p. 3267-3288.

Telford, W.M., L.P. Geldart, and R.E. Sheriff, Applied geophysics. Vol. 1. 1990: Cambridge university press.

Vatankhah, S., V.E. Ardestani, and R.A. Renaut, Automatic estimation of the regularization parameter in 2D focusing gravity inversion: application of the method to the Safo manganese mine in the northwest of Iran. Journal of Geophysics and Engineering, 2014. **11**(4): p. 045001.

APPENDIX A

Phillips *et al.* (2007) used a quadratic surface (Equation A1) that is fitted within a 3×3 windows of data in a least-squares sense and obtained its coefficients.

$$S(x,y) = a x^2 + b y^2 + c x y + d x + e y + f, \quad \text{(A1)}$$

For a quadratic surface, the most positive and negative curvatures can be calculated using its coefficients as follows:

$$K_{pos} = a + b + \sqrt{(a-b)^2 + c^2}, \quad \text{(A2)}$$

$$K_{neg} = a + b - \sqrt{(a-b)^2 + c^2}. \quad \text{(A3)}$$

The most negative and most positive curvatures can be combined into the following equation to get the shape index:

$$SHI = \frac{2}{\pi} \tan^{-1}\left[\frac{K_{neg} + K_{pos}}{K_{neg} - K_{pos}}\right]. \quad \text{(A4)}$$